

MMLANDMARKS: a Cross-View Instance-Level Benchmark for Geo-Spatial Understanding

Oskar Kristoffersen^{1,2} Alba R. Sánchez¹ Morten R. Hannemose^{1,2}

Anders B. Dahl^{1,2} Dim P. Papadopoulos^{1,2}

¹ Technical University of Denmark

² Pioneer Center for AI

{ofhkr, albre, mohan, abda, dimp}@dtu.dk

mmlandmarks.compute.dtu.dk

Abstract

Geo-spatial analysis of our world benefits from a multimodal approach, as every single geographic location can be described in numerous ways (images from various viewpoints, textual descriptions, and geographic coordinates). Current geo-spatial benchmarks have limited coverage across modalities, considerably restricting progress in the field, as current approaches cannot integrate all relevant modalities within a unified framework. We introduce the Multi-Modal Landmark dataset (MMLANDMARKS), a benchmark composed of four modalities: 197k high-resolution aerial images, 329k ground-view images, textual information, and geographic coordinates for 18,557 distinct landmarks in the United States. The MMLANDMARKS dataset has a one-to-one correspondence across every modality, which enables training and benchmarking models for various geo-spatial tasks, including cross-view Ground-to-Satellite retrieval, ground and satellite geolocalization, Text-to-Image, and Text-to-GPS retrieval. We demonstrate broad generalization and competitive performance against off-the-shelf foundational models and specialized state-of-the-art models across different tasks by employing a simple CLIP-inspired baseline, illustrating the necessity for multimodal datasets to achieve broad geo-spatial understanding.

1. Introduction

Recent advances in computer vision have been driven by the availability of large-scale datasets for object detection [17, 40], scene understanding [94, 104], and event recognition [88]. Similarly, geo-spatial understanding has been motivated by the growing availability of worldwide satellite imagery and a call for remote sensing imagery as a distinct modality in machine learning [65]. With the vast amount of foundational remote sensing models [46], many approaches

combine remote sensing information from various locations and resolutions. Multimodality has become a central part of geo-spatial methods, combining data across visual modalities (e.g. multispectral imagery, ground-level views), sensor types (e.g. GPS, LiDAR), and additional modalities like text [16, 49] or audio [19]. However, many foundational models focus on solving coarse, low-resolution tasks such as landcover semantic segmentation or climate-zone classification, falling short for high-resolution understanding [1, 6, 15, 37, 41, 49, 55, 57]. While many aerial and high-resolution satellite datasets exist [34, 81, 93, 97], they are designed for object detection and classification, without providing tasks on an instance level.

Localization is another challenging geo-spatial task where one wants to answer the broad question “Where in the world was this photo taken?”. Several approaches provide novel progress in this field using various modalities. Geo-localization models train on large-scale geotagged datasets derived from YFCC100M [78] or Mapillary [87], intending to directly predict the most accurate GPS location from a query image [5, 14, 27, 28, 53, 61, 82, 83, 89]. While effective at regional scales, models struggle with fine-grained localization due to large intra-class variation caused by viewing angle or time of image capture. Landmark Retrieval at regional [62] or global [56, 90] levels focus on exact landmark matching, but are computationally expensive and not scalable. Visual Place Recognition [9, 10] relaxes the task by classifying images within a certain range of the landmark as positive matches, yet it is still only viable for regional localization. Cross-view localization bridges the large domain gap between ground and aerial perspectives [18, 32, 43, 72, 91, 96, 98, 107–109]. However, datasets heavily depend on Google Street View panoramas, which restrict coverage to roads and urban areas. Due to the lack of image diversity, cross-view benchmarks have become saturated. Furthermore, licensing restrictions on satellite and street-view imagery limit

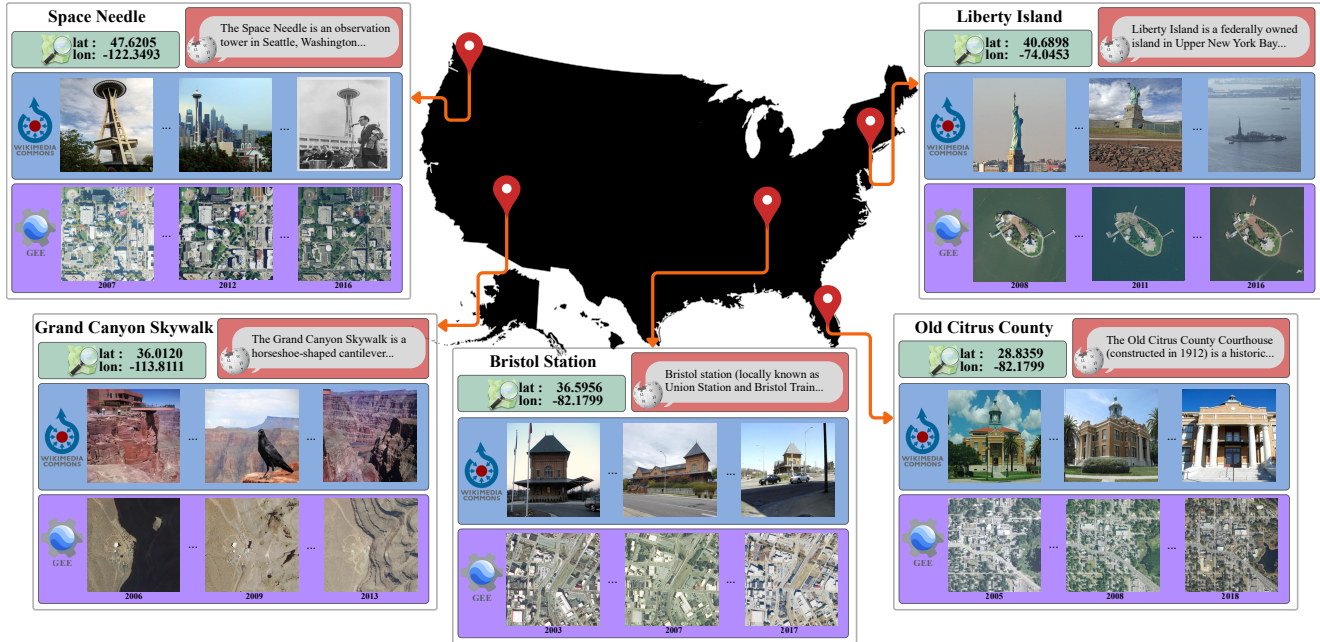


Figure 1. **MMLANDMARKS**. We present four distinct data modalities: ground-view images, aerial imagery, GPS coordinates, and textual descriptions, collected from 18,557 unique landmarks in the United States. Data sources are included alongside each modality.

the scientific research on datasets collected through Google, slowing research involving street-view and satellite imagery [31].

Despite the advances of multimodal methods in remote sensing and localization, a core limitation remains: the lack of fine-grained, instance-level datasets that span multiple modalities and viewpoints. Existing datasets fall short in terms of scale, diversity, or annotation granularity, making it challenging to train models capable of reasoning about specific landmarks and locations across modalities. To address these shortcomings, we introduce **MMLANDMARKS**, a large-scale, instance-level dataset covering 18,557 landmarks across the United States.

MMLANDMARKS is US-only by design, as the National Agriculture Imagery Program (NAIP) [81] is, to our knowledge, the only openly available source of high-resolution aerial imagery with sufficient geographic diversity to support large-scale multimodal geo-spatial research. Other open-access remote sensing resources are either low resolution or cover only small, fragmented regions of the world. Fig. 1 shows some examples of landmarks, while Fig. 2 illustrates the collection process. We leverage the ground-view index set from the Google Landmarks Dataset v2 (GLDV2), from which we remove all landmarks collected in **MMLANDMARKS**, leading to 714k ground images. We also collect a satellite index set with 100k images, and ensure that there is no overlap with the training set. **MMLANDMARKS** is made to push localization as a unified framework where models can be trained and applied to any

downstream geo-spatial task. But also to stimulate multimodal learning in a setting where all modalities are available for each instance in the dataset. To the best of our knowledge, **MMLANDMARKS** is the first dataset with complete one-to-one correspondence across four modalities. It is also the first fine-grained, continental-scale cross-view dataset with permissive licenses that enable the training and sharing of data and models. We summarize our main contributions as follows:

- **MMLANDMARKS dataset.** We collect a new dataset with complete pairwise correspondence across four modalities: ground-view, aerial-view, text information, and GPS coordinates. The dataset contains 329k ground and 197k aerial images from 18,557 unique landmarks (see Sec. 3).
- **Geo-spatial multitasking.** Unlike any other specialized geo-spatial datasets, **MMLANDMARKS** provides a unified framework for training and evaluating models across multiple tasks.
- **Benchmark evaluation.** We report the results of foundational and specialized models on various instance-level geo-spatial tasks and illustrate the potential of training with our dataset by implementing a simple baseline (see Sec. 5).

2. Related Work

Multimodal Learning. CLIP [63] sparked recent progress in multimodal learning, followed by supervised [22, 39] and

Table 1. **Dataset comparison.** Modality abbreviations: *S* - Satellite, *G* - Ground, *T* - Text, *C* - Coordinates, *D* - Drone. In the Scale column, the number in parentheses indicates the number of cities.

Task	Dataset	Year	Train(G/S)	Index(G/S)	Instances	Scale (Cities)	Modalities	Open-access	License
Geo localization	IM2GPS [29]	2008	6.4M/-	-	-	Global	G,C	✗	N/A
	YFCC100M [78]	2016	100M/-	-	-	Global	G,C	✓	Flickr TC
	PlaNet [89]	2016	126M/-	-	-	Global	G,C	✗	N/A
	MP16 [35]	2017	4.7M/-	-	-	Global	G,C	✓	Flickr TC
	OSV-5M [5]	2017	5.1M/-	-	-	Global	G,C	✓	CC-BY-SA
Cross-View Retrieval	CVUSA [91]	2015	35k/35k	8.8k/8.8k	-	USA(1)	G,S	✓	Flickr TC
	Vo. [84]	2016	450k/450k	70k/70k	-	USA(11)	G,S	✓	N/A
	CVACT [43]	2019	44k/44k	92k/92k	-	Australia(1)	G,S	✓	N/A
	Uni-1652 [103]	2020	11.6k/701	5.5k/1652	1652	72 Universities	G,S,D	✓	N/A
	VIGOR [107]	2021	51k/44k	53k/46k	-	USA(4)	G,S	✓	N/A
	CV-Cities [32]	2024	162k/162k	61k/61k	-	Global(16)	G,S	✓	N/A
	CVGlobal [98]	2024	134k/134k	-	-	Global(7)	G,S	✓	N/A
Landmark Retrieval	R-Oxford [62]	2018	-	5k + 1M/-	11	Oxford	G	✓	Flickr TC/CC
	R-Paris [62]	2018	-	6k + 1M/-	11	Paris	G	✓	Flickr TC/CC
	GLDv1 [56]	2018	1.2M/-	1.1M/-	30k	Global	G	✗	Multiple
	GLDv2 [90]	2020	4.1M/-	764k/-	200k	Global	G	✓	CC/Public-domain
	MMLANDMARKS	2025	329k/197k	714k/100k	18,557	USA	G,S,T,C	✓	CC/Public-domain

self-supervised [3, 23, 24, 52, 79] approaches for learning joint representations with two or more distinct modalities [2, 7, 23, 26, 54, 106]. Imagebind [23] and LanguageBind [106] align multiple modalities with image and text anchors, enabling cross-modal associations with no direct supervision. Multimodal representation learning requires large-scale paired datasets, often web-scraped from the internet [23, 63, 78]. Most existing models use image-text pairs, while one-to-one data alignment across multiple modalities remains limited.

In geo-spatial understanding, multimodal learning is also applied for various tasks [16, 19, 33, 82]. WildSat [16] and Geobind [19] use ecological markers to obtain representations of animal habitats [66, 67, 74], while SatCLIP [33] and GeoCLIP [82] leverage geo-tagged ground and aerial imagery for localization [5, 14, 28, 53, 61]. Other efforts rely on open-source multi-spectral satellite and aerial imagery [1, 6, 15, 37, 38, 41, 48, 50, 55, 57, 85] or incorporate language supervision to enhance semantic understanding in remote sensing [47, 49, 70, 95]. In the geo-spatial domain, proposed methods [8, 21, 25, 102] combine remote sensing datasets with aerial [12, 13, 34, 51, 77, 86, 92, 93, 97, 105], and satellite images [30, 44, 68, 75, 76]. While these datasets, combining satellite and aerial images, enable large-scale model training in remote sensing, they typically lack fine-grained, instance-level annotations at high resolution. Unlike most existing models limited to specific modality pairs, MMLANDMARKS supports dense, instance-level supervision across all modality combinations, enabling the learning and evaluation of truly unified geo-spatial models.

Image-to-Image Localization. Accurate localization with limited metadata is the fundamental task of determining the location where a query image was taken through re-

trieval. The task typically involves retrieving the most visually similar image from a large reference database, thereby inferring the geographic position of the query. Early approaches rely on image retrieval techniques for both Ground-to-Ground [4, 9, 29, 56, 62, 64, 90, 99] and Ground-to-Satellite [18, 71, 72, 96, 101, 108, 109] applications. While such methods perform well for large, densely sampled databases, they often depend on robust feature representations and struggle to scale for global localization tasks.

Workman et al. [91] are the first to introduce CVUSA as a cross-view localization benchmark, focusing on locations within the continental United States. Subsequent works expanded this idea by densely collecting similar datasets from various cities and regions [32, 43, 84, 98, 103, 107]. To bridge the substantial domain gap between ground-level panoramas and overhead satellite imagery, many state-of-the-art methods employ geometric transformations or warping techniques, aligning one view to the other [36, 71, 98]. Cross-view benchmarks have become saturated due to the strong geometric correspondence between views and the lack of diversity in image content, which fails to reflect the complexity and variability of real-world scenes [18]. In contrast, MMLANDMARKS addresses these shortcomings by adopting a landmark-centric approach. Rather than relying on road-based panoramas or coarse regional alignment, MMLANDMARKS provides more variation across ground and aerial views by collecting landmark information from OpenStreetMaps [59] and Wikimedia Commons.

Geolocalization addresses the infeasibility of Image-to-Image localization at a global scale by discretizing the Earth into geo-cells [28, 53, 61, 69, 83, 89]. To incorporate information from additional modalities, Haas et al. [27] use CLIP’s text encoder to iteratively predict the most likely

country and city, while Vivanco Cepeda et al. [82] combines CLIP’s image encoder with a GPS encoder. Despite the popularity of direct GPS prediction, geolocalization models typically underperform for fine-grained predictions (< 25 km), since they lack the robust feature comparison used in Image-to-Image retrieval. MMLANDMARKS enables the development and evaluation of models for retrieval-based localization and geolocalization simultaneously by combining cross-view data and GPS coordinates.

3. MMLandmarks Dataset

MMLANDMARKS allows systematic investigation of methods for accurate location prediction using multiple information sources, a capability that current datasets only partially support (see Tab. 1). With more high-resolution satellite images available, cross-view localization becomes a critical step towards unified and globally scalable visual understanding. Combining coordinate prediction from geolocalization models with fine-grained retrieval search in designated areas for prediction refinement can be the way to solve two problems: accurate localization and retrieval at a global scale.

Each data point in MMLANDMARKS is multimodal and exhibits several realistic properties: *Intra-class variability*: The photos collected from Wikimedia Commons inherently contain high variations in lighting conditions, camera angles, and viewpoints, including indoor and outdoor images of the landmarks. The images may also depict other elements indirectly related to the landmarks, such as drawings or scanned documents. *Continent scale*: The dataset offers instance-level cross-view images from the United States. *Long-tailed class distribution*: The number of images per landmark and their geographic location vary significantly depending on the popularity of the landmark. *Temporal change*: The aerial imagery of the National Agriculture Imagery Program enables the collection of high-resolution images of landmarks at various timestamps, providing an additional complexity and a natural augmentation to the dataset, which is rarely found in current remote-sensing datasets.

3.1. Landmark Collection

Finding associations between ground and satellite views of the same instances is a complex task. A straightforward approach is to use Google Maps and Street View to sample satellite views and road panoramas [32, 43, 84, 91, 98, 107]. This cannot be trivially adapted to natural geo-tagged images, since images of a landmark are typically taken from a distance. When sampling the corresponding satellite view, we may end up with no landmark at all since the ground image was taken too far away. Inspired by GLDv2 [90], we leverage the landmarks available in Wikimedia Commons to create a trustworthy correspondence between the ground views and aerial views in MMLANDMARKS.

We collect the meta-information of the United States from OpenStreetMaps [59], and keep all polygons containing at least one of the tags `{wikipedia, wikidata}`. Thereafter, we collect the Wiki-identifier for each polygon from its associated Wikipedia and Wikidata pages. The Wiki-identifier has the format "Q123456" and links all Wiki-information to a single entity. We filter the landmarks and check for the presence of a Wikipedia page containing textual information, and a Wikimedia Commons page containing ground view images associated with the landmark. As a final step, to ensure an even size distribution across all satellite images, we heuristically decide to only keep landmarks where the largest side of their bounding box is less than 400 meters. After the filtration process (see Fig. 2), we obtain 18,557 landmarks in the US with all four modalities.

3.2. Data Collection

In retrieval-based tasks, the goal is to rank images from a large index set according to their similarity with a given query. We construct both a dedicated training set and a large, diverse index set.

Training set. The 329,349 ground images are collected from Wikimedia Commons, which is a large Media Repository containing millions of images licensed under Creative Commons and Public Domain licenses. The images are primarily provided by photographers and organizations, most of which come from yearly Wiki Loves Monuments events. Similar to GLDv2 [90], we resize the images such that the largest side is a maximum of 800 pixels.

We sample aerial images from the publicly available National Agriculture Imagery Program (NAIP) [81], which contains aerial images of the United States with a pixel size of one to two meters. We use Google Earth Engine to collect the images, which provides data for non-commercial and research purposes. For each location, we select aerial images from the years in which they are available, yielding 197,205 aerial images of size 800×800 . Sampling multiple images from the same location adds a new temporal dimension to the aerial modality that is not available in previous cross-view datasets. The aerial imagery contains variations (natural augmentations) resulting from differences in time, weather, angle, sun orientation, and vegetation.

The GPS coordinates of the 18,557 landmarks are set as the center of the landmark, and all text sections from the landmark’s Wikipedia page are collected, while discarding sections such as "References" or "See also".

Index set. To accurately evaluate models, we use two large index sets for Ground-to-Satellite and Satellite-to-Ground retrieval. We use the ground index set from GLDv2 [90], which contains 761k images of 101k landmarks across the world. We filter the landmarks in the index set by country, and find 17,804 belonging in the US. Since the images are sampled similarly to GLDv2 [90], we find all the land-

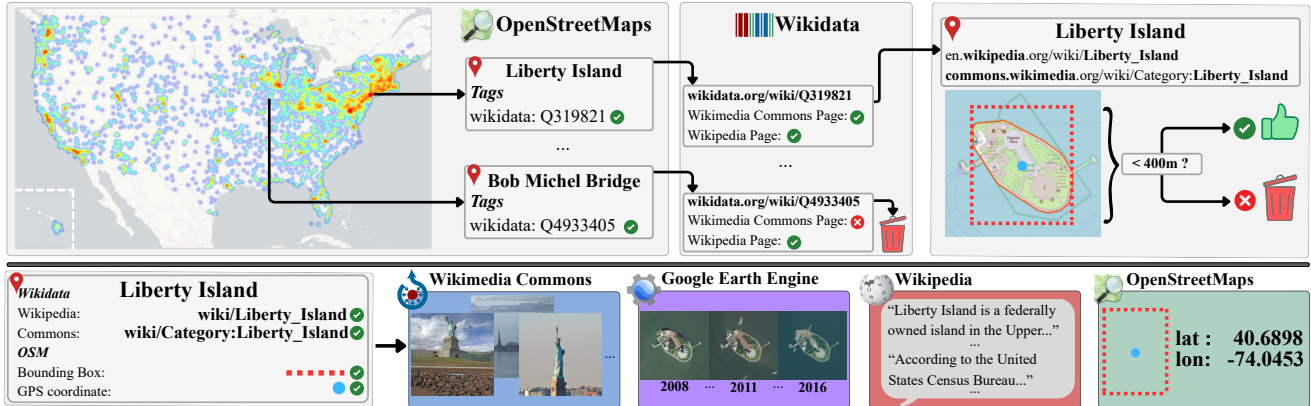


Figure 2. Pipeline for collecting the landmarks with the required criteria. Tags from OpenStreetMaps are used to collect Wiki-identifiers, ensuring that landmarks have a Wikipedia and Wikimedia Commons page. If both are available, we check that the longest edge of the landmark’s bounding box is smaller than 400 meters to keep an even size distribution across the dataset. Every resulting landmark has a Wikimedia Commons page (ground), a Wikipedia page (text), a box size and center (coordinates), and associated aerial imagery (satellite).

marks in the index set that were also collected for the MMLANDMARKS dataset. We remove these 5,277 landmarks found from the index set, yielding a final ground index set of 714,554 images. To avoid a large domain gap between the aerial training and index set, which would make the Ground-to-Satellite retrieval easier, we strategically sample landmarks from the training set by randomly adding some noise to their GPS coordinates until obtaining 100k locations. After ensuring that the new coordinates are more than 500 meters away from any other coordinate in the training set (to avoid seeing a landmark in other images) or any of the 100k index locations, we sample the latest aerial image from these GPS coordinates from the NAIP.

3.3. Data processing

Since the ground images are crowd-sourced images from a street-level viewpoint, they contain both external views of the landmarks (outdoor) and indoor images. However, indoor images may not be appropriate for learning geo-spatial aligned representations. For this reason, we employ a Vision Language Model (llava-hf/llava-1.5-7b-hf) [42] and prompt it to categorize every image as indoor or outdoor. We make a subset of the MMLANDMARKS dataset where only the outdoor images are used, which corresponds to 83% of the original ground views (274,650 outdoor against 54,699 indoor images). To verify the categorization accuracy, 1000 randomly sampled images are reviewed. Only 8.2% of the images are wrongly labelled, most of which are zoomed in or without meaningful context. Further examples and details about the filtering process are provided in the Supplementary Material. In Sec. 5, we train models using all images and a subset with only outdoor images. Unless stated otherwise, both indoor and outdoor images are used.

3.4. Distribution and Challenges

The MMLANDMARKS dataset inherits multiple relevant and realistic challenges from the image collection through Wikimedia Commons and the NAIP. *Skewed distributions*: The landmarks collected are biased in terms of geographical locations and category. As commonly seen in other localization datasets [35, 78], most images from the web are taken in well-known locations, which is also reflected in our dataset (see Fig. 2). There are indeed large concentrations of landmarks around major cities, especially in California and the Northeast. The number of landmarks and images per category also varies significantly, with a large proportion of churches and skyscrapers. *Temporal change*: We take advantage of the vast collection provided by the NAIP to sample aerial images at multiple timestamps, sometimes spanning over a decade. As a consequence, changes may occur both for the landmark and its surroundings. This opens for research in temporal change detection. *Large domain gap*: Learning the correspondence between ground and aerial imagery can become extremely difficult due to large perspective changes from one modality to another. Furthermore, the large intra-class variability in the web collection of ground images makes the task harder, as landmarks may be viewed from a variety of viewpoints, including both indoor and outdoor views of buildings.

3.5. Licenses

All images in MMLANDMARKS are licensed to be used indefinitely. This is an extremely important part of the collection process, since a majority of current cross-view datasets [32, 43, 84, 91, 98, 103, 107] use data that is either restricted in re-distribution or usage for machine learning purposes [31]. The ground view images are licensed under Creative Commons or Public Domain licenses, while the

Table 2. **Cross-view ground and satellite retrieval.** Comparison of median rank (medR, lower is better), mean Average Precision at 1000 (mAP@1k, higher is better), and recall at K ($R@K$, higher is better) between off-the-shelf cross-view Ground-to-Satellite retrieval models and multimodal foundational models on MMLANDMARKS. Median rank is the median position where the first correct match is retrieved. The query and index sizes for satellite to ground are 1000 and 733k respectively, and for ground to satellite are 18,689 and 100k.

model	arch	train res	Satellite → Ground					Ground → Satellite				
			medR ↓	mAP@1k ↑	R@1 ↑	R@5 ↑	R@10 ↑	medR ↓	mAP@1k ↑	R@1 ↑	R@5 ↑	R@10 ↑
DINO [11]	ViT-B	224	84050	0.3	1.3	2.5	3.6	27836	0.6	0.3	1.4	2.2
SigLIP [100]	ViT-B	256	4801	0.8	2.9	7.4	10.3	5437	5.9	4.0	12.0	17.3
SigLIP [100]	ViT-B	384	3854	1.2	2.7	8.7	12.8	4051	7.6	5.3	15.2	20.9
SigLIP [100]	ViT-B	512	5110	1.1	2.8	8.6	12.7	4387	8.0	5.8	15.2	20.6
OAI-CLIP [63]	ViT-B	224	1695	1.4	4.0	11.3	15.8	2215	7.9	5.8	15.2	22.0
SigLIP2 [80]	ViT-B	512	2461	1.8	4.8	10.8	14.4	431	11.7	8.5	21.5	28.6
DiNOv2 [60]	ViT-L	518	28342	0.7	1.9	3.0	4.2	9335	4.7	3.3	8.8	12.5
DiNOv3 [73]	ViT-L	518	14623	1.5	3.7	7.4	10.3	2241	8.5	6.1	15.5	22.3
SigLIP [100]	ViT-L	256	2602	2.0	5.3	11.7	16.7	1302	10.8	8.0	19.1	25.6
SigLIP [100]	ViT-L	384	1546	3.0	7.2	15.2	19.5	679	13.8	10.7	23.8	30.8
OAI-CLIP [63]	ViT-L	336	<u>519</u>	<u>4.9</u>	<u>10.4</u>	<u>21.2</u>	<u>27.5</u>	620	15.2	11.9	26.4	35.2
SigLIP2 [80]	ViT-L	512	682	4.1	8.6	18.6	23.4	<u>140</u>	<u>18.7</u>	<u>14.6</u>	<u>31.6</u>	<u>40.1</u>
Uni-1652 [103]	R50	256	62606	0.1	0.4	0.8	1.3	39961	0.4	0.2	0.9	1.7
Sample4Geo-UNI [18]	ConvNext-B	384	34988	0.4	3.0	6.2	8.0	40056	1.1	0.85	2.8	4.5
MMCLIP	CLIP (ViT-L)	336	23	18.8	30.4	52.4	61.3	48	26.2	20.5	46.5	58.4

aerial images from the NAIP are considered public domain information. We provide all licenses for the collected images as part of MMLANDMARKS, so the dataset users can give the proper attribution when using the images.

4. Training Multimodal Models

We employ a simple yet effective baseline model to learn a shared embedding space across all modalities (i.e., ground-view and aerial-view images, text, and GPS coordinates) of MMLANDMARKS. Our approach enables cross-modal retrieval via nearest neighbor search in the joint space.

Architecture A dedicated encoder processes each modality. We use a frozen CLIP image encoder for both ground and aerial images, the corresponding frozen text encoder for Wikipedia text, and initialize a location encoder following the work from GeoCLIP [82] for GPS coordinates. After each encoder, we add a projection head with two trainable linear layers and a ReLU activation in the middle, following [82]. This allows projecting modality-specific representations to a common dimensionality.

Loss Function To align the modalities, we extend the InfoNCE [58] loss to all pairwise combinations of the four modalities. Given a batch of matching samples across $K = 4$ modalities, the loss is defined as:

$$\mathcal{L} = \frac{1}{K(K-1)} \sum_{i=1}^K \sum_{j=1, j \neq i}^K \mathcal{L}_{i,j} \quad (1)$$

where $\mathcal{L}_{i,j}$ is the contrastive loss between embeddings from modality i and j . During inference, retrieval is performed using k -nearest neighbors in the learned embedding space.

Implementation details We use a pre-trained CLIP ViT-L/14 [20, 63] image encoder for the ground and aerial-view

images, and its text encoder for the Wikipedia text. The location encoder architecture is initialized as in [82] to embed the GPS coordinates. As a simple strategy, we use sentences of each landmark’s text descriptions as inputs for CLIP’s text encoder. We both sample sentences randomly and use the first sentence during training, and compare the results in Tab. 6. All models are trained on a single NVIDIA H100 GPU. All projection layers have a dimension of 512. During training, we keep all encoders frozen except for the location encoder. All models are trained for 20 epochs with an AdamW [45] optimizer, a learning rate of 1×10^{-4} , a weight decay of 5×10^{-4} , and a batch size of 512. During training, we randomly select one ground-view image for each landmark in the minibatch. We experiment with sampling aerial images randomly against always using the latest aerial image available (see Tab. 6). To avoid overfitting, we use a validation set with 1024 landmarks sampled and removed from MMLANDMARKS’s training, and the best model is chosen according to the lowest validation loss. We train with a complete pairwise loss across all modalities and following [63, 82], we set the scaling temperature to 0.07.

5. Experiments

In this section, we evaluate the model trained on MMLANDMARKS and several off-the-shelf state-of-the-art models on several geo-spatial tasks: image-to-image retrieval (Sec. 5.1), ground and satellite geolocalization (Sec. 5.2), and text-to-image/GPS retrieval (Sec. 5.3) to present the cross-modality retrieval capabilities of models trained with MMLANDMARKS. For all tasks, we report performance on the MMLANDMARKS index set. In Sec. 5.4, we analyze design choices of our baseline model.



Figure 3. Text-to-GPS (top 1000), Text-to-Ground and Text-to-Satellite retrieval from the index set with the baseline model. The model accurately locates regions and images that are semantically relevant to the prompt, illustrating strong feature alignment across modalities.

Table 3. **Ground-to-GPS geolocation.** Performance on the MMLANDMARKS query set (18,689 ground images). Ground to Sat to GPS is also done to evaluate cross-view retrieval models.

Method	Distance (% @ km) \uparrow				
	Street (1 km)	City (25 km)	Region (200 km)	Country (750 km)	Continent (2500 km)
Ground \rightarrow Sat \rightarrow GPS					
OAI-CLIP [63](ViT-B/224)	4.06	13.08	19.95	43.68	81.18
OAI-CLIP [63](ViT-L/336)	8.04	23.53	35.50	62.41	86.77
SigLIP2 [80](ViT-L/512)	12.63	24.63	34.44	60.86	89.86
Uni-1652 [103]	0.02	1.15	5.69	22.57	65.52
Sample4Geo-UNI [18]	0.27	2.05	6.86	25.42	66.22
MMCLIP	18.41	37.40	50.99	73.72	91.83
Ground \rightarrow GPS					
Always NYC	0.00	17.73	22.31	47.07	74.86
StreetCLIP [27]	0.53	33.48	48.89	71.29	88.48
osv5m [5]	1.28	13.44	19.19	37.50	57.25
GeoCLIP [82]	21.37	36.44	48.57	71.45	91.50
MMCLIP	16.83	35.95	51.78	74.94	91.52

Table 4. **Satellite-to-GPS geolocation.** Model performance on the MMLANDMARKS query set (1000 satellite images).

Method	Distance (% @ km) \uparrow				
	Street (1 km)	City (25 km)	Region (200 km)	Country (750 km)	Continent (2500 km)
Always NYC	0.0	8.8	15.4	41.7	74.2
StreetCLIP [27]	0.6	27.2	49.6	84.5	93.9
osv5m [5]	0.7	11.1	21.2	44.0	70.8
GeoCLIP [82]	12.3	31.3	48.8	81.3	97.4
MMCLIP	36.9	61.5	81.1	95.5	99.7

5.1. Image-to-Image retrieval

We compare results for cross-view ground and satellite retrieval with foundational and task-specific models (Tab. 2).

Metrics. We adopt the standard Recall@K (R@K) metric, as well as the median rank (medR) for image-to-image retrieval. The Recall values show how often a correct im-

age is retrieved in the first, fifth, and tenth positions from the index set, while the median rank indicates the median position at which the first correct match is retrieved.

Results. All foundation models improve with larger architectures and higher training resolution, while the Uni-1652 and Sample4Geo models adapt poorly to cross-view retrieval on the MMLANDMARKS test set, despite being trained on cross-view benchmarks. All other models use panorama views and often require image pre-processing, making them incompatible in this context. Our baseline model achieves high performance on both retrieval tasks, with a Recall@k that is slightly higher for the Satellite-to-Ground retrieval task.

5.2. Geolocation

Geolocation performance is evaluated on the test set for current models trained exclusively for this task. To reflect a realistic situation, we assume that a given satellite index set typically also includes information about the images’ GPS locations. We evaluate cross-view models for this task, taking the GPS coordinates associated with the first retrieved satellite image as the prediction. As a baseline metric, we take the geographic center of the most densely sampled location in MMLANDMARKS, New York City, and evaluate predicting that location for all queries (“Always NYC”). We report the Ground-to-GPS geolocation, both directly and indirectly (through satellite retrieval), in Tab. 3, and Satellite-to-GPS geolocation in Tab. 4.

Metrics. We follow prior work [28, 82] and use the distance percentage at different kilometer thresholds (Distance(% @ km)). This is the percentage of predictions that fall within a

Table 5. **Text-to-Any retrieval.** Model performance on the MMLANDMARKS query set (1000 first sentences) for Text-to-Satellite and Text-to-GPS retrieval.

Retrieval	medR ↓	mAP@1k ↑	R@1 ↑	R@5 ↑	R@10 ↑
Text → Satellite					
OAI-CLIP (ViT-B/224)	433	15.5	11.6	28.2	38.0
OAI-CLIP (ViT-L/336)	77	27.7	22.2	47.2	60.3
SigLIP2 (ViT-L/512)	3428	6.6	4.5	13.2	18.5
MMCLIP	36	36.2	29.5	62.7	74.4
Text → GPS					
Localization	Street ↑ (1 km)	City ↑ (25 km)	Region ↑ (200 km)	Country ↑ (750 km)	Continent ↑ (2500 km)
MMCLIP	17.6	44.9	71.9	90.7	97.0

specific distance from the true GPS coordinate. We define the GPS index set as the coordinates from the satellite index set, giving a gallery of 100k GPS locations in the United States. The Haversine distance is then computed between the predicted and the ground-truth coordinates as the angular distance between two points on the surface of the Earth.

Results. CLIP [63], SigLIP [80], and the baseline model show promising results in cross-view geolocalization, surpassing direct geolocalization in two metrics and ranking second in the remaining three. The poor performance of cross-view models reflects the lack of diversity in the current benchmarks. StreetCLIP and osv5m serve as baselines, and also perform much worse than GeoCLIP and our baseline model. GeoCLIP performs best only on the Street level and is beaten across all other metrics. With only a fraction of the number of images used to train task-specific models such as GeoCLIP, our baseline trained with MMLANDMARKS performs better across most geolocalization metrics. Since MMLANDMARKS is built on popular landmarks, there is a high chance that ground images from the query and index set also appear in MP16 [35], significantly boosting GeoCLIP’s results. In fact, over 1.2 million images from MP16 were taken in the United States, increasing the chances of overlap.

While cross-view models could be evaluated previously, not all index ground images are geo-tagged. Therefore, for Satellite-to-GPS localization, we only test models that have been trained for geolocalization. Here, the baseline model reflects a clear understanding of the geolocation of satellite imagery. While StreetCLIP and osv5m adapt poorly to the task, GeoCLIP demonstrates a semantic understanding of the query images, albeit with less precision on fine-grained street-level details.

5.3. Text-to-Any Retrieval

We evaluate the baseline model on Text-to-Any retrieval in Tab. 5, by extracting the nearest neighbour features of encoded query first sentences with the index features from the remaining modalities. Text-to-Satellite and GPS perform even better than the best models in Tab. 3. These results stem from the fact that the first Wikipedia sentence

Table 6. **Ablation studies.** Performance for different models trained in various configurations: training objectives, modalities included, text sampling (F: first sentence or R: random sentence), satellite sampling (R: random or L: last), and whether indoor ground images are included during training (Subset). The gray row is our final baseline model, used in all tables.

Objective	Modalities	Text	Sat	Subset	mAP@1k _{S→G}	mAP@1k _{G→S}	G/S→GPS (1 km)
all⇔all	G,S	×	R	×	17.59	25.59	×
	G,S,T	F	R	×	17.31	25.61	×
	G,S,T	R	R	×	17.29	26.16	×
	G,S,C	×	R	×	16.19	22.96	16.67 / 27.9
	G,S,T,C	F	R	×	17.39	25.05	15.63 / 27.7
	G,S,T,C	R	R	×	16.93	24.94	16.27 / 25.4
MMCLIP	G,S,T,C	R	R	✓	17.45	25.07	17.71 / 27.2
	G,S,T,C	R	L	✓	18.79	26.20	16.83 / 36.9
G ⇔ all	G,S,T,C	R	R	×	16.5	24.86	16.55 / 15.7
	G,S,T,C	R	R	✓	17.08	25.16	16.18 / 15.4
	G,S,T,C	R	L	✓	18.89	27.46	15.68 / 18.3

often contains strong geographical cues, such as the city or state of the query landmark. In Fig. 3 we illustrate modality alignment with example text prompts by separately performing Text-to-GPS, Text-to-Ground, and Text-to-Satellite retrieval. We show the first 1000 nearest GPS coordinates, as well as the top six ground and satellite images retrieved.

5.4. Ablation studies

Tab. 6 shows all experiments performed with different contrastive learning objectives, number of modalities, text and satellite sampling strategy, and data filtration. Increasing the number of modalities appears to result in a slight decrease in retrieval performance. Random and First sampling offer equivalent results, while taking the most recent satellite image (L: last) and training on the ground view subset with outdoor images significantly improves the baseline across all tasks. While the Imagebind baseline performs slightly better on retrieval tasks, the fully contrastive setup stands out in geolocalization, especially for Satellite-to-GPS, where the Imagebind baseline’s features are only indirectly aligned.

6. Conclusion

We introduced MMLANDMARKS, a large-scale multimodal dataset aligned at the landmark level across four complementary modalities: ground-view images, high-resolution satellite imagery, Wikipedia text, and GPS coordinates. By enabling one-to-one correspondence between modalities, MMLANDMARKS supports a wide range of geo-spatial tasks under a unified framework, and we show that a simple baseline model can compete and even outperform specialized and foundational vision models in cross-view retrieval, geolocalization, Text-to-Satellite, and Text-to-GPS retrieval. Geospatial learning is of a multimodal nature – we hope that this benchmark will motivate further research in multimodal learning, cross-view reasoning, and geo-spatial understanding of the world.

References

- [1] Peri Akiva, Matthew Purri, and Matthew Leotta. Self-supervised material and texture representation learning for remote sensing tasks. In *Proceedings of the IEEE/CVF Conference on Computer Vision and Pattern Recognition*, pages 8203–8215, 2022. 1, 3
- [2] Jean-Baptiste Alayrac, Adria Recasens, Rosalia Schneider, Relja Arandjelović, Jason Ramapuram, Jeffrey De Fauw, Lucas Smaira, Sander Dieleman, and Andrew Zisserman. Self-supervised multimodal versatile networks. *Advances in neural information processing systems*, 33:25–37, 2020. 3
- [3] Relja Arandjelovic and Andrew Zisserman. Look, listen and learn. In *Proceedings of the IEEE international conference on computer vision*, pages 609–617, 2017. 3
- [4] Relja Arandjelovic, Petr Gronat, Akihiko Torii, Tomas Paždla, and Josef Sivic. Netvlad: Cnn architecture for weakly supervised place recognition. In *Proceedings of the IEEE conference on computer vision and pattern recognition*, pages 5297–5307, 2016. 3
- [5] Guillaume Astruc, Nicolas Dufour, Ioannis Siglidis, Constantin Aronssohn, Nacim Bouia, Stephanie Fu, Romain Loiseau, Van Nguyen Nguyen, Charles Raude, Elliot Vincent, et al. Openstreetview-5m: The many roads to global visual geolocation. In *Proceedings of the IEEE/CVF Conference on Computer Vision and Pattern Recognition*, pages 21967–21977, 2024. 1, 3, 7
- [6] Kumar Ayush, Burak Uzket, Chenlin Meng, Kumar Tanmay, Marshall Burke, David Lobell, and Stefano Ermon. Geography-aware self-supervised learning. In *Proceedings of the IEEE/CVF International Conference on Computer Vision*, pages 10181–10190, 2021. 1, 3
- [7] Alexei Baevski, Wei-Ning Hsu, Qiantong Xu, Arun Babu, Jiatao Gu, and Michael Auli. Data2vec: A general framework for self-supervised learning in speech, vision and language. In *International conference on machine learning*, pages 1298–1312. PMLR, 2022. 3
- [8] Favyen Bastani, Piper Wolters, Ritwik Gupta, Joe Ferdinando, and Aniruddha Kembhavi. Satlaspretrain: A large-scale dataset for remote sensing image understanding. In *Proceedings of the IEEE/CVF International Conference on Computer Vision*, pages 16772–16782, 2023. 3
- [9] Gabriele Berton and Carlo Masone. Megaloc: One retrieval to place them all. In *Proceedings of the Computer Vision and Pattern Recognition Conference*, pages 2861–2867, 2025. 1, 3
- [10] Gabriele Berton, Gabriele Trivigno, Barbara Caputo, and Carlo Masone. Eigenplaces: Training viewpoint robust models for visual place recognition. In *Proceedings of the IEEE/CVF International Conference on Computer Vision*, pages 11080–11090, 2023. 1
- [11] Mathilde Caron, Hugo Touvron, Ishan Misra, Hervé Jégou, Julien Mairal, Piotr Bojanowski, and Armand Joulin. Emerging properties in self-supervised vision transformers. In *Proceedings of the IEEE/CVF international conference on computer vision*, pages 9650–9660, 2021. 6
- [12] Gong Cheng, Junwei Han, and Xiaoqiang Lu. Remote sensing image scene classification: Benchmark and state of the art. *Proceedings of the IEEE*, 105(10):1865–1883, 2017. 3
- [13] Gordon Christie, Neil Fendley, James Wilson, and Ryan Mukherjee. Functional map of the world. In *Proceedings of the IEEE Conference on Computer Vision and Pattern Recognition*, pages 6172–6180, 2018. 3
- [14] Brandon Clark, Alec Kerrigan, Parth Parag Kulkarni, Vicente Vivanco Cepeda, and Mubarak Shah. Where we are and what we’re looking at: Query based worldwide image geo-localization using hierarchies and scenes. In *Proceedings of the IEEE/CVF Conference on Computer Vision and Pattern Recognition*, pages 23182–23190, 2023. 1, 3
- [15] Yezhen Cong, Samar Khanna, Chenlin Meng, Patrick Liu, Erik Rozi, Yutong He, Marshall Burke, David Lobell, and Stefano Ermon. Satmae: Pre-training transformers for temporal and multi-spectral satellite imagery. *Advances in Neural Information Processing Systems*, 35:197–211, 2022. 1, 3
- [16] Rangel Daroya, Elijah Cole, Oisín Mac Aodha, Grant Van Horn, and Subhransu Maji. Wildsat: Learning satellite image representations from wildlife observations. In *Proceedings of the IEEE/CVF International Conference on Computer Vision*, pages 6143–6154, 2025. 1, 3
- [17] Jia Deng, Wei Dong, Richard Socher, Li-Jia Li, Kai Li, and Li Fei-Fei. Imagenet: A large-scale hierarchical image database. In *2009 IEEE conference on computer vision and pattern recognition*. Ieee, 2009. 1
- [18] Fabian Deuser, Konrad Habel, and Norbert Oswald. Sample4geo: Hard negative sampling for cross-view geolocalisation. In *Proceedings of the IEEE/CVF International Conference on Computer Vision*, pages 16847–16856, 2023. 1, 3, 6, 7
- [19] Aayush Dhakal, Subash Khanal, Srikumar Sastry, Adeel Ahmad, and Nathan Jacobs. Geobind: Binding text, image, and audio through satellite images. In *IGARSS 2024-2024 IEEE International Geoscience and Remote Sensing Symposium*, pages 2729–2733. IEEE, 2024. 1, 3
- [20] Alexey Dosovitskiy. An image is worth 16x16 words: Transformers for image recognition at scale. *arXiv preprint arXiv:2010.11929*, 2020. 6
- [21] Alistair Francis and Mikolaj Czerkawski. Major tom: Expandable datasets for earth observation. In *IGARSS 2024-2024 IEEE International Geoscience and Remote Sensing Symposium*, pages 2935–2940. IEEE, 2024. 3
- [22] Rohit Girdhar, Mannat Singh, Nikhila Ravi, Laurens Van Der Maaten, Armand Joulin, and Ishan Misra. Omnivore: A single model for many visual modalities. In *Proceedings of the IEEE/CVF conference on computer vision and pattern recognition*, pages 16102–16112, 2022. 2
- [23] Rohit Girdhar, Alaaeldin El-Nouby, Zhuang Liu, Mannat Singh, Kalyan Vasudev Alwala, Armand Joulin, and Ishan Misra. Imagebind: One embedding space to bind them all. In *Proceedings of the IEEE/CVF conference on computer vision and pattern recognition*, 2023. 3
- [24] Rohit Girdhar, Alaaeldin El-Nouby, Mannat Singh, Kalyan Vasudev Alwala, Armand Joulin, and Ishan Misra.

- Omnimae: Single model masked pretraining on images and videos. In *Proceedings of the IEEE/CVF conference on computer vision and pattern recognition*, pages 10406–10417, 2023. 3
- [25] Xin Guo, Jiangwei Lao, Bo Dang, Yingying Zhang, Lei Yu, Lixiang Ru, Liheng Zhong, Ziyuan Huang, Kang Wu, Dingxiang Hu, et al. Skysense: A multi-modal remote sensing foundation model towards universal interpretation for earth observation imagery. In *Proceedings of the IEEE/CVF Conference on Computer Vision and Pattern Recognition*, 2024. 3
- [26] Andrey Guzhov, Federico Raue, Jörn Hees, and Andreas Dengel. Audioclip: Extending clip to image, text and audio. In *ICASSP 2022-2022 IEEE International Conference on Acoustics, Speech and Signal Processing (ICASSP)*, pages 976–980. IEEE, 2022. 3
- [27] Lukas Haas, Silas Alberti, and Michal Skreta. Learning generalized zero-shot learners for open-domain image geolocalization. *arXiv preprint arXiv:2302.00275*, 2023. 1, 3, 7
- [28] Lukas Haas, Michal Skreta, Silas Alberti, and Chelsea Finn. Pigeon: Predicting image geolocations. In *Proceedings of the IEEE/CVF Conference on Computer Vision and Pattern Recognition*, pages 12893–12902, 2024. 1, 3, 7
- [29] James Hays and Alexei A. Efros. im2gps: estimating geographic information from a single image. In *Proceedings of the IEEE Conf. on Computer Vision and Pattern Recognition (CVPR)*, 2008. 3
- [30] Patrick Helber, Benjamin Bischke, Andreas Dengel, and Damian Borth. Eurosat: A novel dataset and deep learning benchmark for land use and land cover classification. *IEEE Journal of Selected Topics in Applied Earth Observations and Remote Sensing*, 12(7):2217–2226, 2019. 3
- [31] Marco Helbich, Matthew Danish, SM Labib, and Britta Ricker. To use or not to use proprietary street view images in (health and place) research? that is the question. *Health & Place*, 87:103244, 2024. 2, 5
- [32] Gaoshuang Huang, Yang Zhou, Luying Zhao, and Wenjian Gan. Cv-cities: Advancing cross-view geo-localization in global cities. *IEEE Journal of Selected Topics in Applied Earth Observations and Remote Sensing*, 2024. 1, 3, 4, 5
- [33] Konstantin Klemmer, Esther Rolf, Caleb Robinson, Lester Mackey, and Marc Rußwurm. Satclip: Global, general-purpose location embeddings with satellite imagery. In *Proceedings of the AAAI Conference on Artificial Intelligence*, pages 4347–4355, 2025. 3
- [34] Darius Lam, Richard Kuzma, Kevin McGee, Samuel Doolley, Michael Laielli, Matthew Klaric, Yaroslav Bulatov, and Brendan McCord. xvview: Objects in context in overhead imagery. *arXiv preprint arXiv:1802.07856*, 2018. 1, 3
- [35] Martha Larson, Mohammad Soleymani, Guillaume Gravier, Bogdan Ionescu, and Gareth JF Jones. The benchmarking initiative for multimedia evaluation: Mediaeval 2016. *IEEE MultiMedia*, 24(1):93–96, 2017. 3, 5, 8
- [36] Guopeng Li, Ming Qian, and Gui-Song Xia. Unleashing unlabeled data: A paradigm for cross-view geolocalization. In *Proceedings of the IEEE/CVF Conference on Computer Vision and Pattern Recognition*, pages 16719–16729, 2024. 3
- [37] Xuyang Li, Danfeng Hong, and Jocelyn Chanussot. S2mae: A spatial-spectral pretraining foundation model for spectral remote sensing data. In *Proceedings of the IEEE/CVF Conference on Computer Vision and Pattern Recognition*, pages 24088–24097, 2024. 1, 3
- [38] Zhihao Li, Biao Hou, Siteng Ma, Zitong Wu, Xianpeng Guo, Bo Ren, and Licheng Jiao. Masked angle-aware autoencoder for remote sensing images. In *European Conference on Computer Vision*, pages 260–278. Springer, 2024. 3
- [39] Valerii Likhoshesterov, Anurag Arnab, Krzysztof Choromanski, Mario Lucic, Yi Tay, Adrian Weller, and Mostafa Dehghani. Polyvit: Co-training vision transformers on images, videos and audio. *arXiv preprint arXiv:2111.12993*, 2021. 2
- [40] Tsung-Yi Lin, Michael Maire, Serge Belongie, James Hays, Pietro Perona, Deva Ramanan, Piotr Dollár, and C Lawrence Zitnick. Microsoft coco: Common objects in context. In *European conference on computer vision*, pages 740–755. Springer, 2014. 1
- [41] Fan Liu, Delong Chen, Zhangqingyun Guan, Xiacong Zhou, Jiale Zhu, Qiaolin Ye, Liyong Fu, and Jun Zhou. Remoteclip: A vision language foundation model for remote sensing. *IEEE Transactions on Geoscience and Remote Sensing*, 2024. 1, 3
- [42] Haotian Liu, Chunyuan Li, Qingyang Wu, and Yong Jae Lee. Visual instruction tuning. *Advances in neural information processing systems*, 36:34892–34916, 2023. 5, 17
- [43] Liu Liu and Hongdong Li. Lending orientation to neural networks for cross-view geo-localization. In *Proceedings of the IEEE/CVF conference on computer vision and pattern recognition*, pages 5624–5633, 2019. 1, 3, 4, 5
- [44] Yang Long, Gui-Song Xia, Shengyang Li, Wen Yang, Michael Ying Yang, Xiao Xiang Zhu, Liangpei Zhang, and Deren Li. On creating benchmark dataset for aerial image interpretation: Reviews, guidances, and million-aid. *IEEE Journal of selected topics in applied earth observations and remote sensing*, 14:4205–4230, 2021. 3
- [45] Ilya Loshchilov and Frank Hutter. Decoupled weight decay regularization. *arXiv preprint arXiv:1711.05101*, 2017. 6
- [46] Siqi Lu, Junlin Guo, James R Zimmer-Dauphinee, Jordan M Nieusma, Xiao Wang, Steven A Wernke, Yuankai Huo, et al. Vision foundation models in remote sensing: A survey. *IEEE Geoscience and Remote Sensing Magazine*, 2025. 1
- [47] Junwei Luo, Zhen Pang, Yongjun Zhang, Tingzhu Wang, Linlin Wang, Bo Dang, Jiangwei Lao, Jian Wang, Jingdong Chen, Yihua Tan, et al. Skysensegpt: A fine-grained instruction tuning dataset and model for remote sensing vision-language understanding. *arXiv preprint arXiv:2406.10100*, 2024. 3
- [48] Utkarsh Mall, Bharath Hariharan, and Kavita Bala. Change-aware sampling and contrastive learning for satellite images. In *Proceedings of the IEEE/CVF Conference on Computer Vision and Pattern Recognition*, pages 5261–5270, 2023. 3

- [49] Utkarsh Mall, Cheng Perng Phoo, Meilin Kelsey Liu, Carl Vondrick, Bharath Hariharan, and Kavita Bala. Remote sensing vision-language foundation models without annotations via ground remote alignment. *arXiv preprint arXiv:2312.06960*, 2023. 1, 3
- [50] Oscar Manas, Alexandre Lacoste, Xavier Giró-i Nieto, David Vazquez, and Pau Rodriguez. Seasonal contrast: Unsupervised pre-training from uncurated remote sensing data. In *Proceedings of the IEEE/CVF International Conference on Computer Vision*, pages 9414–9423, 2021. 3
- [51] Aaron Maxwell, Timothy Warner, Brian Vanderbilt, and Christopher Ramezan. Land cover classification and feature extraction from national agriculture imagery program (naip) orthoimagery: A review. *Photogrammetric Engineering & Remote Sensing*, 83:737–747, 2017. 3
- [52] Pedro Morgado, Nuno Vasconcelos, and Ishan Misra. Audio-visual instance discrimination with cross-modal agreement. In *Proceedings of the IEEE/CVF conference on computer vision and pattern recognition*, pages 12475–12486, 2021. 3
- [53] Eric Muller-Budack, Kader Pustu-Iren, and Ralph Ewerth. Geolocation estimation of photos using a hierarchical model and scene classification. In *Proceedings of the European conference on computer vision (ECCV)*, pages 563–579, 2018. 1, 3
- [54] Arsha Nagrani, Paul Hongsuck Seo, Bryan Seybold, Anja Hauth, Santiago Manen, Chen Sun, and Cordelia Schmid. Learning audio-video modalities from image captions. In *European Conference on Computer Vision*, pages 407–426. Springer, 2022. 3
- [55] Vishal Nedungadi, Ankit Kariryaa, Stefan Oehmcke, Serge Belongie, Christian Igel, and Nico Lang. Mmearth: Exploring multi-modal pretext tasks for geospatial representation learning. In *European Conference on Computer Vision*, pages 164–182. Springer, 2024. 1, 3
- [56] Hyeonwoo Noh, Andre Araujo, Jack Sim, Tobias Weyand, and Bohyung Han. Large-scale image retrieval with attentive deep local features. In *Proceedings of the IEEE international conference on computer vision*, pages 3456–3465, 2017. 1, 3
- [57] Mubashir Noman, Muzammal Naseer, Hisham Cholakkal, Rao Muhammad Anwer, Salman Khan, and Fahad Shahbaz Khan. Rethinking transformers pre-training for multi-spectral satellite imagery. In *Proceedings of the IEEE/CVF Conference on Computer Vision and Pattern Recognition*, pages 27811–27819, 2024. 1, 3
- [58] Aaron van den Oord, Yazhe Li, and Oriol Vinyals. Representation learning with contrastive predictive coding. *arXiv preprint arXiv:1807.03748*, 2018. 6
- [59] OpenStreetMap contributors. Openstreetmap. <https://www.openstreetmap.org>, 2024. 3, 4
- [60] Maxime Oquab, Timothée Darcet, Théo Moutakanni, Huy Vo, Marc Szafraniec, Vasil Khalidov, Pierre Fernandez, Daniel Haziza, Francisco Massa, Alaaeldin El-Nouby, et al. Dinov2: Learning robust visual features without supervision. *arXiv preprint arXiv:2304.07193*, 2023. 6
- [61] Shraman Pramanick, Ewa M Nowara, Joshua Gleason, Carlos D Castillo, and Rama Chellappa. Where in the world is this image? transformer-based geo-localization in the wild. In *European Conference on Computer Vision*, pages 196–215. Springer, 2022. 1, 3
- [62] Filip Radenović, Ahmet Iscen, Giorgos Tolias, Yannis Avrithis, and Ondřej Chum. Revisiting oxford and paris: Large-scale image retrieval benchmarking. In *Proceedings of the IEEE conference on computer vision and pattern recognition*, pages 5706–5715, 2018. 1, 3
- [63] Alec Radford, Jong Wook Kim, Chris Hallacy, Aditya Ramesh, Gabriel Goh, Sandhini Agarwal, Girish Sastry, Amanda Askell, Pamela Mishkin, Jack Clark, et al. Learning transferable visual models from natural language supervision. In *International conference on machine learning*, pages 8748–8763. PmlR, 2021. 2, 3, 6, 7, 8
- [64] Elias Ramzi, Nicolas Audebert, Clément Rambour, André Araujo, Xavier Bitot, and Nicolas Thome. Optimization of rank losses for image retrieval. *IEEE Transactions on Pattern Analysis and Machine Intelligence*, 2025. 3, 16
- [65] Esther Rolf, Konstantin Klemmer, Caleb Robinson, and Hannah Kerner. Mission critical—satellite data is a distinct modality in machine learning. *arXiv preprint arXiv:2402.01444*, 2024. 1
- [66] Srikumar Sastry, Subash Khanal, Aayush Dhakal, Di Huang, and Nathan Jacobs. Birdsat: Cross-view contrastive masked autoencoders for bird species classification and mapping. In *Proceedings of the IEEE/CVF Winter Conference on Applications of Computer Vision*, pages 7136–7145, 2024. 3
- [67] Srikumar Sastry, Subash Khanal, Aayush Dhakal, Adeel Ahmad, and Nathan Jacobs. Taxabind: A unified embedding space for ecological applications. In *2025 IEEE/CVF Winter Conference on Applications of Computer Vision (WACV)*, pages 1765–1774. IEEE, 2025. 3
- [68] Michael Schmitt, Lloyd Haydn Hughes, Chunping Qiu, and Xiao Xiang Zhu. Sen12ms—a curated dataset of georeferenced multi-spectral sentinel-1/2 imagery for deep learning and data fusion. *arXiv preprint arXiv:1906.07789*, 2019. 3
- [69] Paul Hongsuck Seo, Tobias Weyand, Jack Sim, and Bohyung Han. Cplanet: Enhancing image geolocation by combinatorial partitioning of maps. In *Proceedings of the European Conference on Computer Vision (ECCV)*, pages 536–551, 2018. 3
- [70] Akashah Shabbir, Mohammed Zumri, Mohammed Benamoun, Fahad S Khan, and Salman Khan. Geopixel: Pixel grounding large multimodal model in remote sensing. *arXiv preprint arXiv:2501.13925*, 2025. 3
- [71] Yujiao Shi, Liu Liu, Xin Yu, and Hongdong Li. Spatial-aware feature aggregation for cross-view image based geolocation. *Advances in Neural Information Processing Systems*, 32, 2019. 3
- [72] Yujiao Shi, Xin Yu, Dylan Campbell, and Hongdong Li. Where am i looking at? joint location and orientation estimation by cross-view matching. In *Proceedings of the IEEE/CVF Conference on Computer Vision and Pattern Recognition*, pages 4064–4072, 2020. 1, 3
- [73] Oriane Siméoni, Huy V Vo, Maximilian Seitzer, Federico Baldassarre, Maxime Oquab, Cijo Jose, Vasil Khalidov,

- Marc Szafraniec, Seungeun Yi, Michaël Ramamonjisoa, et al. Dinov3. *arXiv preprint arXiv:2508.10104*, 2025. 6
- [74] Samuel Stevens, Jiaman Wu, Matthew J Thompson, Elizabeth G Campolongo, Chan Hee Song, David Edward Carlyn, Li Dong, Wasila M Dahdul, Charles Stewart, Tanya Berger-Wolf, et al. Bioclip: A vision foundation model for the tree of life. In *Proceedings of the IEEE/CVF conference on computer vision and pattern recognition*, pages 19412–19424, 2024. 3
- [75] Gencer Sumbul, Marcela Charfuelan, Begüm Demir, and Volker Markl. Bigearthnet: A large-scale benchmark archive for remote sensing image understanding. In *IGARSS 2019 - 2019 IEEE International Geoscience and Remote Sensing Symposium*. IEEE, 2019. 3
- [76] Gencer Sumbul, Arne De Wall, Tristan Kreuziger, Filipe Marcelino, Hugo Costa, Pedro Benevides, Mario Caetano, Begüm Demir, and Volker Markl. Bigearthnet-mm: A large-scale, multimodal, multilabel benchmark archive for remote sensing image classification and retrieval [software and data sets]. *IEEE Geoscience and Remote Sensing Magazine*, 9(3):174–180, 2021. 3
- [77] Xian Sun, Peijin Wang, Zhiyuan Yan, Feng Xu, Ruiping Wang, Wenhui Diao, Jin Chen, Jihao Li, Yingchao Feng, Tao Xu, et al. Fair1m: A benchmark dataset for fine-grained object recognition in high-resolution remote sensing imagery. *ISPRS Journal of Photogrammetry and Remote Sensing*, 184:116–130, 2022. 3
- [78] Bart Thomee, David A. Shamma, Gerald Friedland, Benjamin Elizalde, Karl Ni, Douglas Poland, Damian Borth, and Li-Jia Li. Yfcc100m: the new data in multimedia research. *Communications of the ACM*, 59(2):64–73, 2016. 1, 3, 5
- [79] Yonglong Tian, Dilip Krishnan, and Phillip Isola. Contrastive multiview coding. In *Computer Vision–ECCV 2020: 16th European Conference, Glasgow, UK, August 23–28, 2020. Proceedings, Part XI 16*, pages 776–794. Springer, 2020. 3
- [80] Michael Tschannen, Alexey Gritsenko, Xiao Wang, Muhammad Ferjad Naeem, Ibrahim Alabdulmohsin, Nikhil Parthasarathy, Talfan Evans, Lucas Beyer, Ye Xia, Basil Mustafa, et al. Siglip 2: Multilingual vision-language encoders with improved semantic understanding, localization, and dense features. *arXiv preprint arXiv:2502.14786*, 2025. 6, 7, 8
- [81] USDA Farm Production and Conservation - Business Center, Geospatial Enterprise Operations. NAIP: National Agriculture Imagery Program (USDA/NAIP/DOQQ). <https://naip-usdaonline.hub.arcgis.com/>. 1, 2, 4
- [82] Vicente Vivanco Cepeda, Gaurav Kumar Nayak, and Mubarak Shah. Geoclip: Clip-inspired alignment between locations and images for effective worldwide geolocalization. *Advances in Neural Information Processing Systems*, 36:8690–8701, 2023. 1, 3, 4, 6, 7
- [83] Nam Vo, Nathan Jacobs, and James Hays. Revisiting im2gps in the deep learning era. In *Proceedings of the IEEE international conference on computer vision*, pages 2621–2630, 2017. 1, 3
- [84] Nam N Vo and James Hays. Localizing and orienting street views using overhead imagery. In *European conference on computer vision*, pages 494–509. Springer, 2016. 3, 4, 5
- [85] Di Wang, Jing Zhang, Bo Du, Gui-Song Xia, and Dacheng Tao. An empirical study of remote sensing pretraining. *IEEE Transactions on Geoscience and Remote Sensing*, 61: 1–20, 2022. 3
- [86] Syed Waqas Zamir, Aditya Arora, Akshita Gupta, Salman Khan, Guolei Sun, Fahad Shahbaz Khan, Fan Zhu, Ling Shao, Gui-Song Xia, and Xiang Bai. isaid: A large-scale dataset for instance segmentation in aerial images. In *Proceedings of the IEEE/CVF conference on computer vision and pattern recognition workshops*, pages 28–37, 2019. 3
- [87] Frederik Warburg, Soren Hauberg, Manuel Lopez-Antequera, Pau Gargallo, Yubin Kuang, and Javier Civera. Mapillary street-level sequences: A dataset for lifelong place recognition. In *Proceedings of the IEEE/CVF conference on computer vision and pattern recognition*, pages 2626–2635, 2020. 1
- [88] Ethan Weber, Dim P Papadopoulos, Agata Lapedriza, Ferda Ofli, Muhammad Imran, and Antonio Torralba. Incidents1m: a large-scale dataset of images with natural disasters, damage, and incidents. *IEEE transactions on pattern analysis and machine intelligence*, 2022. 1
- [89] Tobias Weyand, Ilya Kostrikov, and James Philbin. Planet-photo geolocation with convolutional neural networks. In *Computer Vision–ECCV 2016: 14th European Conference, Amsterdam, The Netherlands, October 11–14, 2016. Proceedings, Part VIII 14*, pages 37–55. Springer, 2016. 1, 3
- [90] Tobias Weyand, Andre Araujo, Bingyi Cao, and Jack Sim. Google landmarks dataset v2-a large-scale benchmark for instance-level recognition and retrieval. In *Proceedings of the IEEE/CVF conference on computer vision and pattern recognition*, pages 2575–2584, 2020. 1, 3, 4
- [91] Scott Workman, Richard Souvenir, and Nathan Jacobs. Wide-area image geolocalization with aerial reference imagery. In *IEEE International Conference on Computer Vision (ICCV)*, 2015. 1, 3, 4, 5
- [92] Gui-Song Xia, Jingwen Hu, Fan Hu, Baoguang Shi, Xiang Bai, Yanfei Zhong, Liangpei Zhang, and Xiaoqiang Lu. Aid: A benchmark data set for performance evaluation of aerial scene classification. *IEEE Transactions on Geoscience and Remote Sensing*, 55(7):3965–3981, 2017. 3
- [93] Gui-Song Xia, Xiang Bai, Jian Ding, Zhen Zhu, Serge Belongie, Jiebo Luo, Mihai Datcu, Marcello Pelillo, and Liangpei Zhang. Dota: A large-scale dataset for object detection in aerial images. In *Proceedings of the IEEE conference on computer vision and pattern recognition*, pages 3974–3983, 2018. 1, 3
- [94] Jianxiong Xiao, James Hays, Krista A Ehinger, Aude Oliva, and Antonio Torralba. Sun database: Large-scale scene recognition from abbey to zoo. In *2010 IEEE computer society conference on computer vision and pattern recognition*. IEEE, 2010. 1
- [95] Linrui Xu, Ling Zhao, Wang Guo, Qiujuan Li, Kewang Long, Kaiqi Zou, Yuhan Wang, and Haifeng Li. Rs-gpt4v: A unified multimodal instruction-following dataset

- for remote sensing image understanding. *arXiv preprint arXiv:2406.12479*, 2024. 3
- [96] Hongji Yang, Xiufan Lu, and Yingying Zhu. Cross-view geo-localization with layer-to-layer transformer. *Advances in Neural Information Processing Systems*, 34: 29009–29020, 2021. 1, 3
- [97] Yi Yang and Shawn Newsam. Bag-of-visual-words and spatial extensions for land-use classification. In *Proceedings of the 18th SIGSPATIAL international conference on advances in geographic information systems*, pages 270–279, 2010. 1, 3
- [98] Junyan Ye, Zhutao Lv, Weijia Li, Jinhua Yu, Haote Yang, Huaping Zhong, and Conghui He. Cross-view image geo-localization with panorama-bev co-retrieval network. In *European Conference on Computer Vision*, pages 74–90. Springer, 2024. 1, 3, 4, 5
- [99] Shuhe Yokoo, Kohei Ozaki, Edgar Simo-Serra, and Satoshi Iizuka. Two-stage discriminative re-ranking for large-scale landmark retrieval. In *Proceedings of the IEEE/CVF Conference on Computer Vision and Pattern Recognition Workshops*, pages 1012–1013, 2020. 3
- [100] Xiaohua Zhai, Basil Mustafa, Alexander Kolesnikov, and Lucas Beyer. Sigmoid loss for language image pre-training. In *Proceedings of the IEEE/CVF international conference on computer vision*, pages 11975–11986, 2023. 6
- [101] Xiaohan Zhang, Xingyu Li, Waqas Sultani, Chen Chen, and Safwan Wshah. Geodtr+: toward generic cross-view geolocalization via geometric disentanglement. *IEEE Transactions on Pattern Analysis and Machine Intelligence*, 2024. 3
- [102] Zilun Zhang, Tiancheng Zhao, Yulong Guo, and Jianwei Yin. Rs5m and georsclip: A large scale vision-language dataset and a large vision-language model for remote sensing. *IEEE Transactions on Geoscience and Remote Sensing*, 2024. 3
- [103] Zhedong Zheng, Yunchao Wei, and Yi Yang. University-1652: A multi-view multi-source benchmark for drone-based geo-localization. In *Proceedings of the 28th ACM international conference on Multimedia*, pages 1395–1403, 2020. 3, 5, 6, 7
- [104] Bolei Zhou, Agata Lapedriza, Aditya Khosla, Aude Oliva, and Antonio Torralba. Places: A 10 million image database for scene recognition. *IEEE transactions on pattern analysis and machine intelligence*, 2017. 1
- [105] Weixun Zhou, Shawn Newsam, Congmin Li, and Zhenfeng Shao. Patternnet: A benchmark dataset for performance evaluation of remote sensing image retrieval. *ISPRS Journal of Photogrammetry and Remote Sensing*, 145:197–209, 2018. 3
- [106] Bin Zhu, Bin Lin, Munan Ning, Yang Yan, Jiayi Cui, Hongfa Wang, Yatian Pang, Wenhao Jiang, Junwu Zhang, Zongwei Li, et al. Languagebind: Extending video-language pretraining to n-modality by language-based semantic alignment. *arXiv preprint arXiv:2310.01852*, 2023. 3
- [107] Sijie Zhu, Taojiannan Yang, and Chen Chen. Vigor: Cross-view image geo-localization beyond one-to-one retrieval. In *Proceedings of the IEEE/CVF Conference on Computer Vision and Pattern Recognition*, pages 3640–3649, 2021. 1, 3, 4, 5
- [108] Sijie Zhu, Mubarak Shah, and Chen Chen. Transgeo: Transformer is all you need for cross-view image geo-localization. In *Proceedings of the IEEE/CVF Conference on Computer Vision and Pattern Recognition*, pages 1162–1171, 2022. 3
- [109] Yingying Zhu, Hongji Yang, Yuxin Lu, and Qiang Huang. Simple, effective and general: A new backbone for cross-view image geo-localization. *arXiv preprint arXiv:2302.01572*, 2023. 1, 3

MMLANDMARKS: a Cross-View Instance-Level Benchmark for Geo-Spatial Understanding

Supplementary Material

We provide additional information and visualizations for the MMLANDMARKS dataset. Sec. A describes the distribution of images per landmark, geographic and categoric distributions, and details the collection pipeline for selecting the landmarks with OpenStreetMaps, Wikimedia Commons and Wikipedia. In Sec. B, more visualizations of the dataset are included, with bounding box examples and a more detailed analysis of each modality illustrated with landmarks from Denver in Figures 10 and 11. The VLM data processing procedure is mentioned in Sec. C, with examples of when the VLM fails to correctly categorise the images in Fig. 9. Finally, additional illustrations of landmarks from MMLANDMARKS are presented in Figures 12-15.

Algorithm 1 MMLANDMARKS landmark collection pipeline

Require: *OSM* data information, Wikidata, Wikimedia Commons, Wikipedia

- 1: $Dataset = \{\}$
- 2: **for** each sample $poly\!ygon_i$ in *OSM* **do**
- 3: $(lat, lon) = nodes(poly\!ygon_i)$
- 4: **if** $(wikidata \cup wikipedia) \in poly\!ygon_i$ tags **then**
- 5: Extract Wiki information Q_i .
- 6: $(Commons_i \& Wikipedia_i) \leftarrow wikidata.org/wiki/Q_i$
- 7: **if** $\exists(\text{ground images}) \in Commons_i$ **then**
- 8: $G_i = True$
- 9: **end if**
- 10: **if** $\exists(\text{wiki text}) \in Wikipedia_i$ **then**
- 11: $T_i = True$
- 12: **end if**
- 13: **if** $abs(min(lat) - max(lat)) \cap abs(min(lon) - max(lon)) < 400m$ **then**
- 14: $S_i = True$
- 15: $C_i = True$
- 16: **end if**
- 17: **end if**
- 18: $MML_i = \{G_i, T_i, S_i, C_i\}$
- 19: **if** $\{M_i = True \mid \forall M_i \in MML_i\}$ **then**
- 20: $Dataset \leftarrow MML_i$
- 21: **end if**
- 22: **end for**
- 23: *Dataset* contains US landmarks with ground, satellite, text, and GPS information.

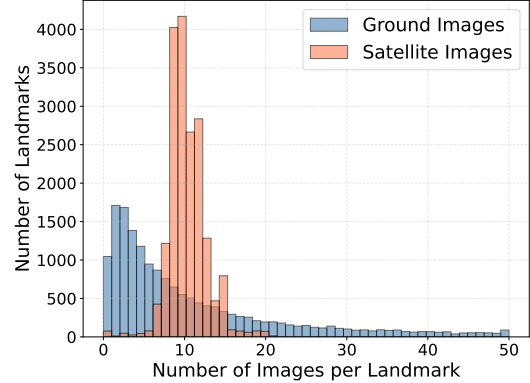


Figure 4. Histogram distribution of the number of images per landmark. A large proportion of landmarks have between 1 and 10 ground images, with a long-tailed distribution. The number of satellite images per landmark follows a bell curve centred at 10 images, with some landmarks having up to 20 aerial images.

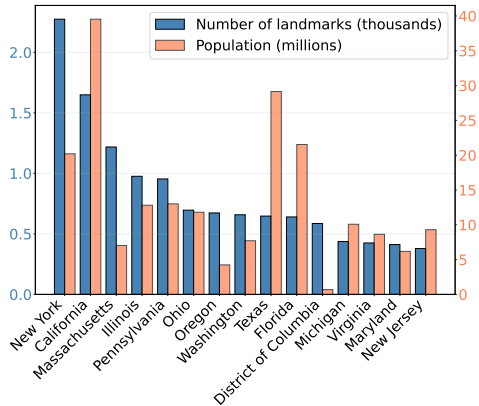
A. Dataset Details

Distribution. As mentioned in Sec. 3, the data contains long-tail distributions, both in terms of geographical location, landmark type, and number of images per landmark. In this section, we provide additional information and illustrate these characteristics of the datasets that are inherent in geo-spatial data.

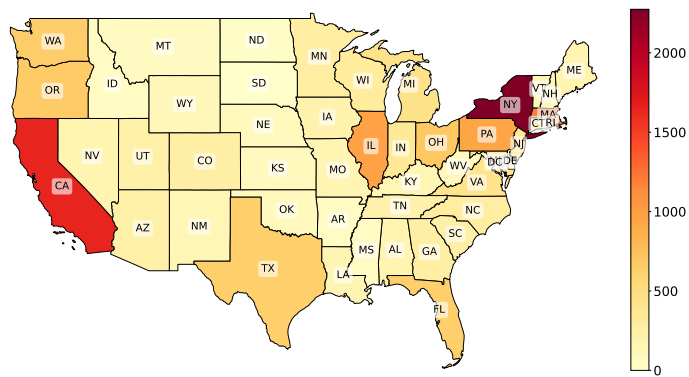
In Fig. 4, the number of images per landmark is plotted for ground and satellite images. The ground images have a long tail, with most landmarks having 1 to 10 images. The satellite images have a normal distribution, with an average of 10 images per landmark, and some have as many as 20 images, spanning over two decades.

The histogram in Fig. 5 shows the top 15 states with the most landmarks in blue, as well as the population of each state in orange. The number of landmarks does not correlate with the population of the state, with a clear example of the District of Columbia (a federal district which is not part of any state), where many governmental landmarks are located despite a low number of residents. The states with the lowest number of landmarks are Hawaii (22), South Dakota (35), and North Dakota (37).

On the right of Fig. 5, a map of the United States illustrates the geographic distribution of landmarks by state, showing the highest concentrations in states with larger populations, such as New York, California, Texas, and Florida.



(a) Histogram distribution of the top 15 states with the most landmarks (blue), compared to each state’s population (orange). The two distributions diverge, with certain states being disproportionately over-represented or under-represented.



(b) Geographic visualization of the number of landmarks per state in the United States. similar to (a), a large proportion of landmarks come from popular areas such as New York & California.

Figure 5. Visual and Geographical illustrations of the landmark distribution across MMLANDMARKS.

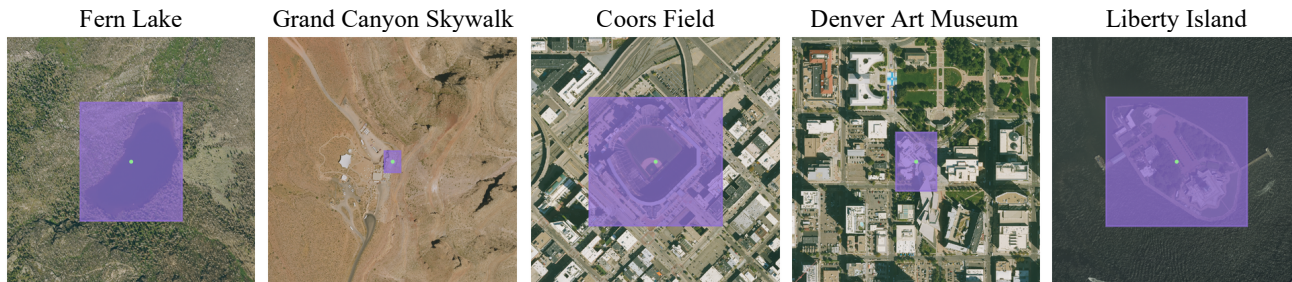


Figure 6. Visualization of the center GPS (green) and bounding boxes (purple) for the polygons associated with different landmarks.

Collection pipeline. In Alg. 1, we present our landmark collection pipeline for MMLANDMARKS. For each polygon found from OpenStreetMaps (*OSM*), we filter those that have either a `wikidata` or `wikipedia` tag in their description. This grants us the possibility to search for the landmark’s Wiki-identifier ($Q_i = Q123456$), from which the landmark’s Wikipedia and Wikimedia Commons webpage can be retrieved.

If ground images and Wikipedia text are available, we proceed to the final part of the processing pipeline: aerial uniformity. We aim to streamline the collection process from the National Agricultural Imagery Program (NAIP) while ensuring that all images have consistent dimensions. In fact, many landmarks vary in size and shape, sometimes spanning several kilometers (e.g., lakes, railways, mountain ranges, etc.). The scarcity of such large landmarks would cause geospatial ambiguity: to capture the entire landmark, one may need to sample images from a small zoom level, leading to low-resolution imagery. Alternatively, samples from various locations of the landmark at high resolution could be a direction. However, this approach often results

Licenses	Counts
CC BY	70,288
CC SA	85
CC BY-SA	181,409
CC BY-NC-SA	76
Public Domain	56,216
CC0	16,046
Attribution	873
No restrictions	3,902

Table 7. Specific licenses for the ground view images in MMLANDMARKS. The licenses and link to each image are also included as part of the dataset for proper attribution.

in a predominance of uniform images depicting only rocks, water, or small portions of a building.

This both complicates the pipeline and incurs ambiguity due to the lack of correspondence between the modalities. To this end, we heuristically choose a maximum length of 400 meters for the largest side of the landmark’s bounding

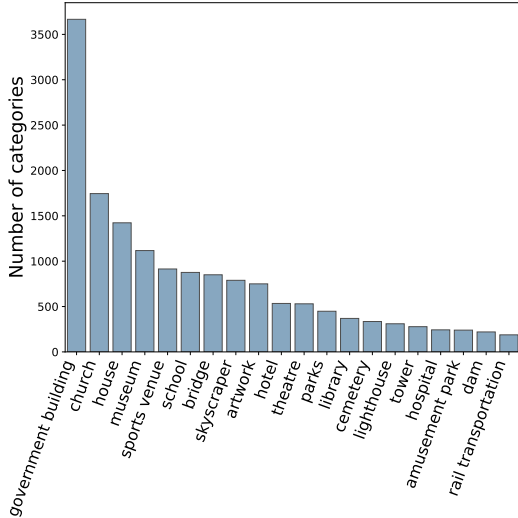


Figure 7. 15 most popular super-categories in MMLANDMARKS. Each landmark is categorized as one of the 79 hierarchical super-categories from Ramzi et al. [64]. There is a large majority of “government building” landmarks, which are further analysed in Fig. 8.

box. As mentioned in Sec. 3, the ground images are resized such that the largest side is 800 pixels. Keeping the same pixel dimensions, we aim to sample aerial images of pixel size 800×800 . After visual inspections, we find that 400 meters yields a balance between the landmark and its surroundings.

Licenses. We collect the MMLANDMARKS dataset, intending to make everything freely accessible and usable. The NAIP aerial imagery is categorized as Public Domain, making it ideal for data collection and incurring no significant filtration in the process. For ground-view images sourced from Wikimedia Commons, an additional step is required to verify the licensing of each image. We keep all the images licensed under “Creative Commons”, “Public Domain”, and other licenses such as “Attribution” and “No restrictions” which allow copy, modification and redistribution. We group the licenses and summarize their count in Tab. 7.

B. Additional Visualizations

Super-categories. As extra information retrieved from each landmark’s Wikidata page, we collect tags under the “Instance of” section for all landmarks as their category, similar to the Hierarchical GLDV2 [64], in which 79 unique hierarchical super-categories are defined. Once the tags are found, we use a CLIP text encoder to embed each category and assign it to one of the super-categories from Ramzi et al. [64]. This is achieved by computing the logits between the 79 super-category embeddings and each query category,

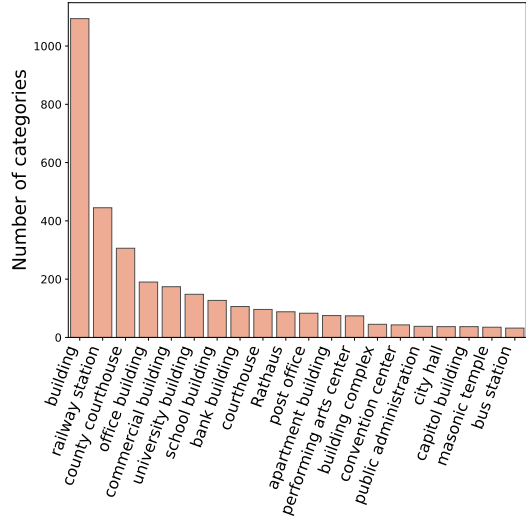


Figure 8. 15 most popular categories from the “government building” super-category. Since a CLIP text encoder is used to classify each category amongst one of the 79 hierarchical categories, all landmark categories with the tag “building” are placed under “government building”.

then selecting the super-category with the highest probability. In Fig. 7, we show the number of landmarks per super-category. Because of the large proportion of landmarks identified as “government building”, we also illustrate the sub-categories of the top super-category (see Fig. 8). We can see that since a lot of landmarks are simply labelled as “building”, when grouped, they are placed under the “government building” label.

More examples. We show the diversity in MMLANDMARKS by providing examples of landmarks in Fig. 10, as well as temporal changes in the collected aerial imagery in Fig. 11. We illustrate the intra-state diversity by showing landmarks located around Denver, Colorado.

Figure 10 illustrates the diversity of images associated with each landmark, a characteristic typical of web-sourced imagery. For example, in the case of “Coors Field”, ground-level photos include views captured before the game (image 2), during the game (images 3–7), and after the game (image 1), exhibiting variations in camera angle and lighting conditions. The “Denver Art Museum” ground views also include scanned documents (image 8) and art from the museum (image 4). Even more intriguing are images 2 and 3 from the Red Rocks Amphitheatre, where the second image is a postcard version from the landmark, from the same angle as the third image. Finally, the last landmark, “Denver Union Station”, reflects the diverse angles and locations from which images are taken of the same landmark, which together give a full understanding of the landmark and its surroundings. Fig. 10 also illustrates the geo-spatial fine

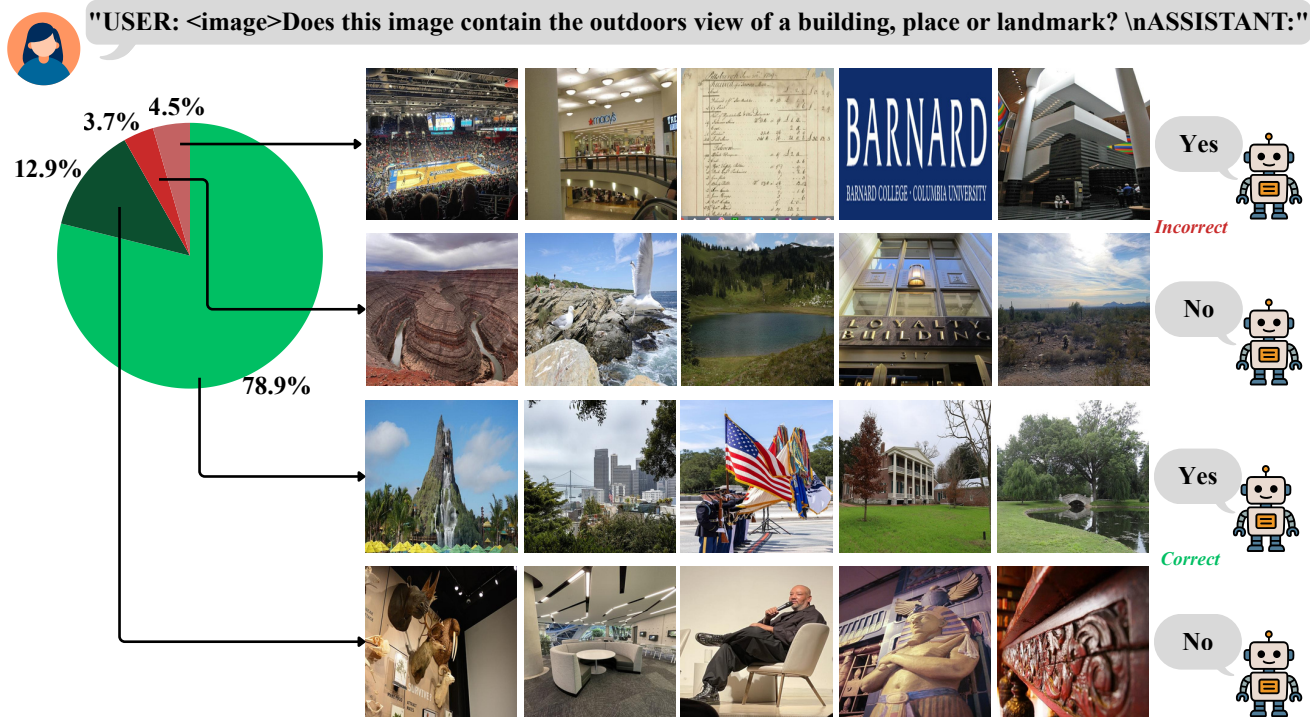


Figure 9. VLM Filtering: Examples of wrong categorizations during the VLM - indoor/outdoor filtering stage. The model may incorrectly classify images as belonging to the opposite category due to visual ambiguities in the images. five examples are shown from the 8.2% wrongly classified ground images in the 1000 visually inspected samples.

granularity by providing accurate GPS locations, along with long textual descriptions of the landmark.

Similarly, in Fig. 11, the aerial images taken from the NAIP illustrate the diversity of the same location when inspecting the same place through time. Not only are all images different in terms of capture time, angle, sun orientation, and season, but physical changes also happen, which can be detected by comparing the images together. Most obvious is the “Fern Lake”, where the size and color of the water vary. It is also evident that tree density was significantly higher in the older (top) images compared to the newer (bottom) views. The fourth image seems to show traces of the wildfires, which have burnt down a majority of the surrounding trees.

In columns one and four, clear changes appear in the surroundings, with a building appearing in the top left corner of the Coors Field images between images 2 and 3, or a parking space being removed between images 4 and 5.

For the “Red Rocks Amphitheatre”, an asphalt parking lot was added between the times when images 1 and 2 were captured. Additionally, the top of the Amphitheatre is now covered by a greyish roof, which is also visible in ground-level images found through a web search for the landmark. The MMLANDMARKS is extremely diverse in terms of geography, textual, visual, and temporal complexity. We show

additional examples of our dataset in Figures 12-15. MMLANDMARKS offers the possibility to train and evaluate models in a unified framework that more realistically reflects our world.

C. VLM Data Processing

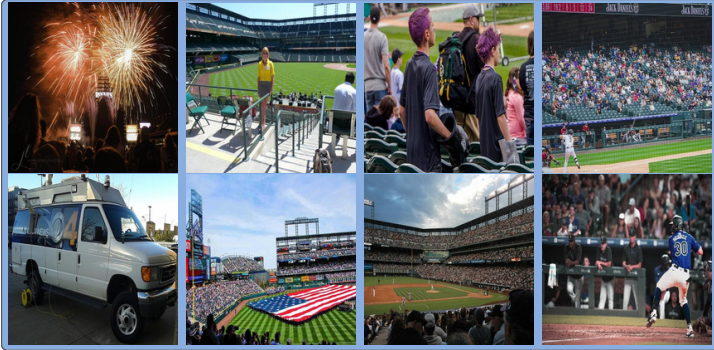
In Fig. 9, we show the splitting process used to create the subset with only outdoor images (83% of the ground images classified as outdoors, as mentioned in Sec. 3. We use a Vision Language Model (llava-hf/llava-1.5-7b-hf) [42] and prompt the following: “USER: <image> Does this image contain the outdoors view of a building, place or landmark?\n ASSISTANT:”. The VLM’s answering window is made very small, such that the VLM only replies by “Yes” (outdoors) or “No” (indoors). In doing so, we remove all images where there are no obvious cues in the image that depict the landmark seen from the exterior. After all images are processed, we sample 1000 ground views randomly and manually inspect them for soundness. We find that 8.2% are wrongly classified, with 3.7% wrongly categorised as indoors, and 4.5% wrongly categorised as outdoors.

However, the 3.7% that are wrongly classified as indoors and should have been marked as outdoors are actually relevant to filter out, since they are often close-up, natural im-

ages that do not provide any particular information about the landmark, and would therefore not contribute during training had they been correctly labelled. This is reflected in the bottom row of Fig. 9, where the VLM classifies a close view of a building or natural landscapes where it cannot see any noticeable landmark, as “No” landmark.

For the images from an indoor setting that are incorrectly classified as “outdoors”, many wrong conclusions from the model stem from basketball courts, malls, or the interior of large buildings that share similar architecture as outdoor landmarks (respectively seen in the top row of Fig. 9: images one, two, and five). Some scanned documents and paintings of buildings are also falsely classified as outdoor images. Upon inspection, we conclude that the number of wrong classifications is acceptably low. The results for models trained on the outdoors subset and presented in Tab. 6 also demonstrate the relevance of employing such a filtration process as a pre-processing clean-up of the raw MMLANDMARKS dataset.

Coors Field



Lat: 39.7560 Lon: -104.9940

Introduction:
 Coors Field is a baseball stadium in downtown Denver, Colorado, United States. It is the ballpark of Major League Baseball's Colorado Rockies. Opened in 1995, the park is located in Denver's Lower Downtown neighborhood, two blocks from Union Station. The stadium has a ...

Construction:
 Coors Field was the first new stadium added in a six-year period in which Denver's sports venues were upgraded, along with Ball Arena ...

...

Denver Art Museum



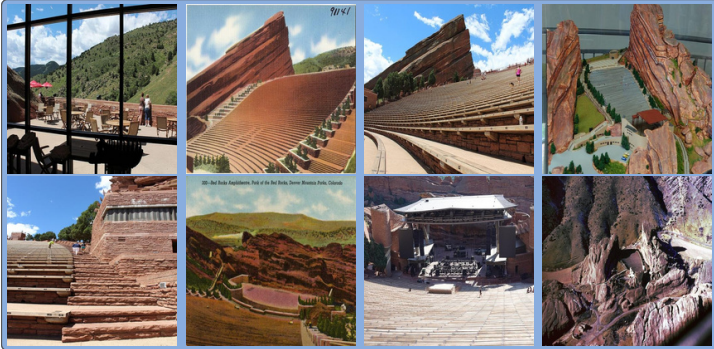
Lat: 39.7373 Lon: -104.9896

Introduction:
 The Denver Art Museum (DAM) is an art museum located in the Civic Center of Denver, Colorado. With an encyclopedic collection of more than 70,000 diverse works from across the centuries and world, the DAM is one of the largest art museums between the West Coast and Chicago. It is known for its ...

1893–1923:
 The museum's origins can be traced back to the founding of the Denver Artists Club in 1893. The Club renamed itself the Denver Art Association in ...

...

Red Rocks Amphitheatre



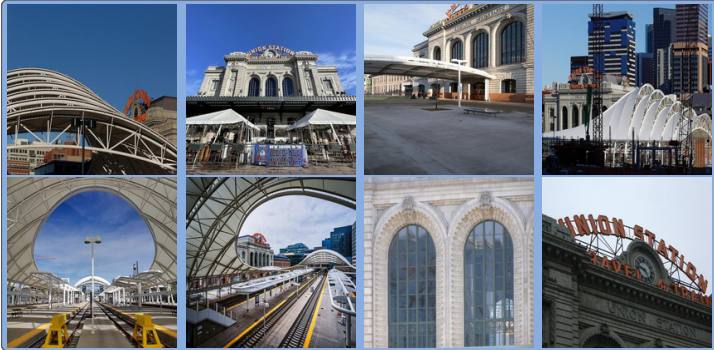
Lat: 39.6654 Lon: -105.2057

Introduction:
 Red Rocks Amphitheatre (also known colloquially as simply Red Rocks) is an open-air amphitheater in the western United States near Morrison, Colorado, approximately ten miles (16 km) southwest of Denver. It is owned and operated by the city of Denver. In addition to several other large sandstone ...

History:
 The natural features surrounding the amphitheater were formed millions of years ago as part of the Fountain Formation, then lifted and tilted during a geological upheaval ...

...

Denver Union Station



Lat: 39.7532 Lon: -105.0003

Introduction:
 Denver Union Station is the main railway station and central transportation hub in Denver, Colorado. It is located at 17th and Wynkoop Streets in the present-day LoDo district and includes the historic station house, a modern open-air train shed, a 22-gate underground bus station, and light rail station. A station ...

19th century: Original structures:
 Denver's first train station was constructed in 1868 to serve the new Denver Pacific Railway, which connected Denver to the main transcontinental line at Cheyenne, Wyoming. By 1875 ...

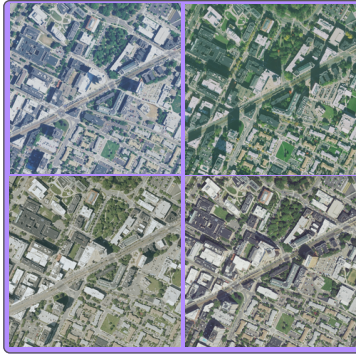
...

Figure 10. Additional examples of landmarks from MMLANDMARKS. The four landmarks are sampled from around Denver, Colorado.



Figure 11. Visual diversity in the aerial imagery from landmarks in MMLANDMARKS. The images are arranged chronologically, ranging from older images at the top to newer images at the bottom. More images of the landmarks are included in the dataset, which are not presented here. The landmarks are sampled from around Denver, Colorado. The temporal aspect of the dataset augments the instance with different moments of capture, angle, and weather conditions. Zoom in to see fine-grained changes in the urban surroundings of columns 1, 2, and 5.

West High School (Salt Lake City) Massachusetts College of Art



Lat: 42.3366 Lon: -71.0988

Introduction:
 Massachusetts College of Art and Design, branded as MassArt, is a public college of visual and applied art in Boston, Massachusetts. Founded in 1873, it is one of the nation's oldest art schools, and the only publicly funded independent art school in the United States. It was the first art college in ...
Campus:
 MassArt is headquartered at 621 Huntington Avenue in Boston, Massachusetts, and occupies a trapezoidal block of old and new buildings it has acquired over the last two decades. Most ...
 ...

West Union Baptist Church



Lat: 40.7746 Lon: -111.9004

Introduction:
 West High School is a public high school in Salt Lake City, Utah. A part of the Salt Lake City School District, the school serves students in the western part of the city. Founded in 1890 as Salt Lake High School, it is among one of the oldest public high schools in Utah. As of 2024, the school is housed in its historic ...
Manual and technical training:
 Beginning with the 1902–1903 school year, the local board of education established manual training. This training was meant to offer practical skills and vocational training, as ...
 ...

The Mount Lenox



Lat: 45.5737 Lon: -122.9070

Introduction:
 West Union Baptist Church is a Baptist congregation and historic church structure in West Union, Oregon, United States.
History:
 The Baptist congregation was founded in 1844 and met in the home of pioneer David Thomas Lenox until 1853, when he donated 2 acres (8,100 m2) of his land for a church and cemetery. The one-story, Classical Revival style building was built of hand-sawn lumber on what is now West Union Road for a little over \$1,500. The 30- by 40-foot (12 m) structure has cedar ...
 ...



Lat: 42.3310 Lon: -73.2820

Introduction:
 The Mount (1902) is a country house in Lenox, Massachusetts, the home of noted American author Edith Wharton, who designed the house and its grounds and considered it her "first real home."
 The estate, located in The Berkshires, is open to the public. The property was declared a National Historic Landmark ...
Paranormal activity:
 In 1942 The Mount became part of the Foxhollow School for Girls, and residents reported unexplained noises and experiences in the living areas of the mansion. Following the school's ...
 ...

Figure 12. Additional examples from the MMLANDMARKS dataset. We illustrate the diversity in the dataset by randomly sampling landmarks. We show sample ground and satellite views, as well as the exact GPS location and parts of the textual descriptions.

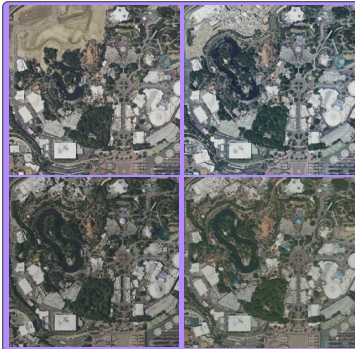
321 North Clark



Lat: 41.8883 Lon: -87.6306

Introduction:
 321 North Clark at Riverfront Plaza is a 35-story, 155.45 m (510.0 ft) skyscraper constructed from 1983 to 1987 in Chicago, Illinois, United States. The tower was built by BCE Development Properties and designed by Skidmore, Owings & Merrill as part of the Riverfront Plaza development on the north bank of the Chicago River. 321 North Clark opened in April 1987 and was named "city development of the year" by the Chicago Sun-Times. The building was originally named Quaker Tower after its anchor tenant, the Quaker Oats Company ...

Golden Horseshoe Saloon

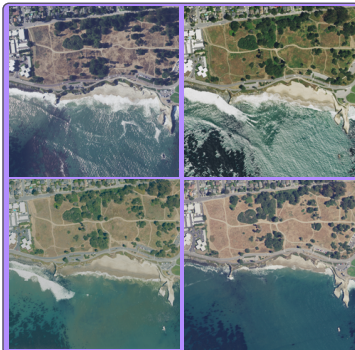


Lat: 33.8119 Lon: -117.9202

Introduction:
 The Golden Horseshoe Saloon (referred to as Pecos Bill's Golden Horseshoe Saloon during construction) is a restaurant and attraction at Disneyland Park in Anaheim, California in the United States. It opened in 1955 with several other original attractions at Disneyland Park. Over the years the venue has housed ...

History:
 The Golden Horseshoe Stage unofficially opened on July 13, 1955, as the Golden Horseshoe Saloon, when Walt and Lillian Disney, along with dozens of guests, celebrated ...

Lighthouse Field State Beach



Lat: 36.9518 Lon: -122.0298

Introduction:
 Lighthouse Field State Beach is a protected beach in the state park system of California, United States. It is located in the city of Santa Cruz at the north end of Monterey Bay. The beach overlooks the Steamer Lane surfing hotspot. It also contains the Santa Cruz Surfing Museum, housed in a 1967 ...

Natural history:
 Lighthouse Field State Beach is a wintering ground for migrating monarch butterflies. Other resident animals include California sea lions and American black swifts.

Malibu Hindu Temple



Lat: 34.0951 Lon: -118.7099

Introduction:
 Malibu Hindu Temple is a Hindu temple in located in the Santa Monica Mountains, in the city of Calabasas near Malibu, California. Built in 1981 and dedicated to the Hindu deity Venkateswara, it features traditional South Indian style and serves as a centre for Hindu worship and cultural events in Southern ...

Architecture and Deities:
 The complex has two temples – the upper temple with Venkateswara as the presiding deity and the lower temple with Shiva as the presiding deity. Both temples are constructed ...

Figure 13. Additional examples from the MMLANDMARKS dataset. We illustrate the diversity in the dataset by randomly sampling landmarks. We show sample ground and satellite views, as well as the exact GPS location and parts of the textual descriptions.



Figure 14. Additional examples from the MMLANDMARKS dataset. We illustrate the diversity in the dataset by randomly sampling landmarks. We show sample ground and satellite views, as well as the exact GPS location and parts of the textual descriptions.

Manta SeaWorld San Diego



Lat: 32.7665 Lon: -117.2273

Introduction:
Manta is a steel launched roller coaster at SeaWorld in San Diego, California, United States. The ride was manufactured by MACK Rides and opened to the public on May 26, 2012. It utilizes the same ride system that was used in Blue Fire which opened in 2009 at Europa Park.

Ride:
Manta features two launches. Riders reach speeds of up to 43 miles per hour (69 km/h) on the two-minute, 2,800-foot (850 m) long ride. The ride stands at a height of 30 feet (9.1 m) and ...

...

Vero Beach Museum of Art



Lat: 27.6499 Lon: -80.3669

Introduction:
The Vero Beach Museum of Art is located at 3001 River Park Drive, Vero Beach, Florida. It houses regional, state and national art exhibits. The Vero Beach Museum of Art is the principal cultural arts facility of its kind on Florida's Treasure Coast. The accredited art museum includes are exhibitions, studio art and ...

History:
Since 1991, the Vero Beach Museum of Art has been recognized by the State of Florida and the Florida Arts Council as a significant cultural establishment through grant awards and ...

...

Warm Water Cove



Lat: 37.7540 Lon: -122.3833

Introduction:
Warm Water Cove is an outdoor, formerly industrialized picnic area in San Francisco, California, located near Pier 80 and the Dogpatch neighborhood. The park contains works of graffiti art, abandoned warehouses, and punk concerts. Free, all-ages shows are set up a few times every month by local Bay Area and touring musicians. Along with 924 Gilman Street, it is one of a few punk rock venues in the Bay Area where D.I.Y. music is performed. The park underwent some cleanup and renovation in 2007.

Woodstock School (Oregon)



Lat: 45.4821 Lon: -122.6124

Introduction:
Woodstock Elementary School, formerly known as Woodstock School, is an elementary school within Portland Public Schools, located in the Woodstock neighborhood of southeast Portland, Oregon, United States. Established in 1891, the school was housed in a four-room building until it joined School District ...

Architecture:
Woodstock School exhibits Classical Revival architecture; elements include entablature, Tuscan-style corner boards with pilasters, and a water table. The building is roughly E-shaped ...

...

Figure 15. Additional examples from the MMLANDMARKS dataset. We illustrate the diversity in the dataset by randomly sampling landmarks. We show sample ground and satellite views, as well as the exact GPS location and parts of the textual descriptions.